ACS APPLIED MATERIALS & INTERFACES

Research Article

www.acsami.org

High Performance of Low Band Gap Polymer-Based Ambipolar Transistor Using Single-Layer Graphene Electrodes

Jong Yong Choi,[†,‡,□] Woonggi Kang,[§,□] Boseok Kang,[∥] Wonsuk Cha,[⊥] Seon Kyoung Son,[†] Youngwoon Yoon,[†] Hyunjung Kim,[⊥] Youngjong Kang,[‡] Min Jae Ko,[†,#] Hae Jung Son,[†,∇] Kilwon Cho,[∥] Jeong Ho Cho,*[,§] and BongSoo Kim*[,†,○]

[†]Photo-electronic Hybrids Research Center, Korea Institute of Science and Technology (KIST), Hwarangno14-gil 5, Seongbuk-gu, Seoul 136-791, Republic of Korea

[‡]Department of Chemistry, Hanyang University, 222 Wangsimni-ro, Seongdong-gu, Seoul 133-791, Republic of Korea

[§]SKKU Advanced Institute of Nanotechnology (SAINT), School of Chemical Engineering, Sungkyunkwan University, 2066, Seobu-ro, Jangan, Suwon-si, Gyeonggi-do 440-746, Republic of Korea

[∥]Department of Chemical Engineering, Pohang University of Science and Technology, Pohang, Gyeong-buk 790-784, Republic of Korea

[⊥]Department of Physics, Sogang University, 35 Baekbeom-ro, Mapo-gu, Seoul 121-742, Republic of Korea

[#]Green School (School of Energy and Environment), Korea University, 1, Anam-dong 5-ga, Seongbuk-gu, Seoul 136-701, Republic of Korea

[∇]Nanomaterials Science and Engineering, Korea University of Science & Technology, Daejeon 305-350, Republic of Korea

[○]Department of Science Education, Ewha Womans University, Seoul 120-750, Republic of Korea

Supporting Information

ABSTRACT: Bottom-contact bottom-gate organic field-effect transistors (OFETs) are fabricated using a low band gap pDTTDPP-DT polymer as a channel material and single-layer graphene (SLG) or Au source/drain electrodes. The SLG-based ambipolar OFETs significantly outperform the Au-based ambipolar OFETs, and thermal annealing effectively improves the carrier mobilities of the pDTTDPP-DT films. The difference is attributed to the following facts: (i) the thermally annealed pDTTDPP-DT chains on the SLG assume more crystalline features with an edge-on orientation as compared to the polymer chains on the Au, (ii) the morphological features of the thermally annealed pDTTDPP-DT films on the SLG electrodes are closer to the features of those on the gate dielectric layer, and (iii) the SLG electrode provides a flatter, more hydrophobic surface that is favorable for the polymer crystallization than the Au. In addition, the preferred carrier transport in each electrode-based OFET is associated with the HOMO/LUMO alignment relative to the Fermi level of the employed electrode. All of these experimental results consistently explain why the carrier mobilities of the SLG-based OFET are more than 10 times higher than those of the Au-based OTFT. This work demonstrates the strong dependence of ambipolar carrier transport on the source/drain electrode and annealing temperature.

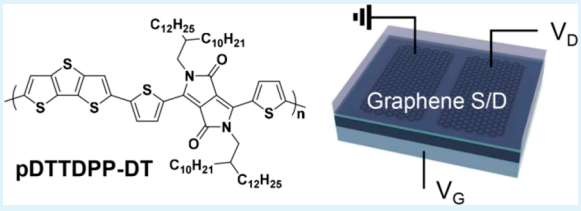

KEYWORDS: *ambipolar organic field-effect transistor, single layer graphene electrode, high carrier mobility, low band gap polymer, film crystallinity*

1. INTRODUCTION

The development of high-performance ambipolar organic field-effect transistors (OFETs) that selectively transport holes or electrons, depending on the bias polarity, is of significant interest for use in complementary metal oxide-semiconductor (CMOS)-like logic circuits and light-emitting transistors.[1−4] Recently, several groups have reported impressive single carrier mobilities using donor−acceptor-type low band gap (LBG) polymers and have spurred efforts toward the synthesis of a variety of donor−acceptor-type LBG polymers. Such polymers are composed of alternating electron-rich donors, such as thiophenes[5,6] and selenophenes,[7−9] and electron-deficient acceptors, such as isoindigos,[10−14] diketopyrrolopyrroles (DPPs),[8,15−17] benzothiadiazoles,[13,18] thiadiazolopyridine,[19−21] and naphthalenedicarboximide.[3,22−24] The performances of ambipolar OFETs comprising semiconducting polymers, on the other hand, remain relatively poor as compared to the performances of single carrier OFETs.[1,14,25] The mobilities of

Received: January 26, 2015
Accepted: March 3, 2015
Published: March 3, 2015

DOI: 10.1021/acsami.5b00747
ACS Appl. Mater. Interfaces 2015, 7, 6002−6012

the ambipolar OFETs may potentially be further enhanced through research into the design of both the polymer backbones and the solubilizing groups.[26,27] The planar conformation and presence of effective linkages between the orbitals of aromatic rings in the polymer backbone have been carefully considered in an effort to control the HOMO/LUMO energy levels and polymer packing structure for achieving optimal hole and electron injection and transport.[18,28] The type and length of substituted alkyl chains were found to affect the device performance, based on studies of a series of structurally fine-tuned DPP-based polymers.[5,29,30] Furthermore, the device fabrication methods require further development. Although thermal annealing has been commonly applied to spin-coated polymer films, solution shearing methods have recently been touted as an effective approach to forming aligned nanofibrillar films.[15,19,21,25] For instance, a DPP-based LBG polymer film processed by applying the solution-shearing method yielded high hole and electron mobilities of 8.84 and 4.34 cm/(V·s), respectively.[25] The addition of high boiling point solvent additives, such as 1-chloronaphthalene, can also improve the OFET performance.[31]

In addition to these studies of the molecular structures and the fabrication processes, device architectures, especially involving contact metals, must be optimized to improve the ambipolar transport performance. Practical considerations for fabricating OFET arrays favor the use of bottom-contact source/drain electrodes, which are amenable to lithographic processes. To date, ambipolar OFETs based on donor−acceptor-type polymers have almost exclusively used Au as the source/drain metals, in either top-contact or bottom-contact geometries. The bottom-contact Au metals can form a step-like barrier at the interface between the Au metals and the semiconducting films and also can induce the different growth of organic semiconductor films on the electrode and of those on the channel region. Such structures may generate poor contacts and charge carrier traps that reduced the charge injection efficiency.[32] Therefore, alternative electrode materials that permit low physical steps and the continuous growth of semiconducting polymers over the electrode and channel regions must be developed for use in ambipolar OFETs.

Recently, one-atom-thick single-layer graphene (SLG) attracted attention as an alternative electrode material for use in OFETs. The SLG provides good transparency, mechanical flexibility, and environmental stability.[33−36] High-quality large-area graphene with a specific thickness may be readily synthesized using chemical vapor deposition (CVD) methods.[35] A few research groups have utilized CVD-grown graphene films as source/drain electrodes in OFETs. Such OFETs displayed good performance and high hole-transporting properties using small molecules of pentacene[37,38] and triethylsilylethynylanthradithiophene.[39] The performance improvements were mainly attributed to the favorable interactions between the aromatic small molecules, which were favorably orientated and highly crystalline, and the top surfaces of the graphene-based contact electrodes. Moreover, the graphene electrode provided efficient electron injection into the semiconducting channel due to its low work function (as compared to the work function of Au). Despite the beneficial attributes of the graphene electrodes, no reports have yet described the application of graphene electrodes in LBG polymer-based OFETs. Graphene could potentially act as an effective source/drain electrode in an ambipolar OFET. Therefore, it is both interesting and important to understand the process by which semiconducting polymer films form on graphene electrodes and the energetic level alignment between the HOMO/LUMO levels of the LBG polymers with respect to the Fermi level of the electrodes for practical application of the graphene-based electrodes in OFETs.

Here, we have characterized the specific interactions between low band gap polymer chains and SLG source/drain electrodes. A low band gap polymer semiconductor, poly(2,5-bis(2-decyltetradecyl)-3-(5-(dithieno[3,2-*b*:2′,3′-*d*]thiophen-2-yl)-thiophen-2-yl)-6-(thiophen-2-yl)-2,5-dihydropyrrolo[3,4-*c*]-pyrrole-1,4-dione) (pDTTDPP-DT), which is a polymer containing alternating electron-rich dithienothiophene (DTT) units and electron-deficient dihydropyrrolopyrroledione (DPP) units, was synthesized and used to fabricate SLG-based ambipolar OFET devices. Au electrode-based devices were also fabricated for comparison. The SLG electrode-based device performance was superior to the performances of the Au electrode-based devices. These results were attributed to the improved polymer chain stacking and edge-on orientation of the polymer chains on the SLG electrode surface. The carrier mobilities were further enhanced by thermal annealing. The optimized ambipolar OFETs prepared with SLG electrodes exhibited average hole and electron mobilities of 1.38 and 2.82 $cm^2\ V^{-1}\ s^{-1}$, respectively. Overall, this work demonstrates the dramatic enhancement in the electrical performances of ambipolar LBG-based OFETs by employing CVD-grown SLG source/drain electrodes.

2. EXPERIMENTAL SECTION

2.1. Synthesis and Characterization of pDTTDPP-DT. 3,6-Bis(5-bromothiophen-2-yl)-2,5-bis(2-decyltetradecyl)pyrrolo[3,4-*c*]-pyrrole-1,4(2*H*,5*H*)-dione (400 mg, 0.3535 mmol), 2,6-bis-(trimethyltin)dithieno[3,2-*b*:2′,3′-*d*]thiophene (188.4 g, 0.3535 mmol), and tetrakis(triphenylphosphine)palladium(0) ($Pd(PPh_3)_4$) (12.3 mg, 0.0106 mmol) were added in a reaction tube, and three vacuum-pumping and argon-venting cycles were conducted. Degassed toluene (7 mL) and dimethylformamide (0.7 mL) were added to the reaction mixture. The reaction solution was stirred and heated gradually from room temperature to 110 °C over 1 h. The viscosity of the mixture was increased significantly, and the color of the reaction mixture turned to green after 3 h. After the reaction mixture was cooled, it was precipitated in methanol. Precipiated crude polymers were collected in a thimble, and Soxhlet extaction was conducted with methanol, acetone, hexane, dichloromethane, and chloroform. The chloroform faction were precipitated in methanol and collected to obtain high molecular weight pDTTDPP-DT. Yield 73% (0.301 g). ^{1}H NMR (400 MHz, $CDCl_3$) δ 8.32−9.79 (b, 2H), 6.45−7.78 (b, 4H), 2.82−4.59 (b, 8H), 0.68−1.77 (b, 124H). GPC (DCB, 80 °C) M_n = 680 kDa, M_w = 1737 kDa, PDI = 2.55 with a low fraction of M_n = 5.8 kDa, M_w = 9.3 kDa, PDI = 1.60.

2.2. OFET Fabrication and Measurement. Ambipolar OFETs based on pDTTDPP-DT were fabricated on a substrate comprising a highly doped n-type Si wafer onto which a 300 nm thick silicon oxide (SiO_2) layer had been thermally grown. The wafer served as the gate electrode. The thermally grown 300 nm thick SiO_2 layer acted as a gate dielectric after the modifying the SiO_2 layer surface with octadecyltrichlorosilane (ODTS, Gelest, Inc.) to reduce electron trapping by the silanol groups on the SiO_2. Prior to treating the SiO_2 surface, the wafer was cleaned in piranha solution for 30 min at 100 °C and washed with copious amounts of distilled water and dried. The water contact angle of the ODTS-treated surfaces was 112°. Separately, high-quality SLG was synthesized on a Cu foil (25 μm, Alfa Aesar), as described previously. The graphene source/drain patterns were defined by photolithography and oxygen plasma etching (~2 s) of SLG layers on a Cu foil. PMMA was then spin-coated at 3500 rpm for 30 s onto the patterned SLG electrodes on a Cu foil. The

DOI: 10.1021/acsami.5b00747
ACS Appl. Mater. Interfaces 2015, 7, 6002−6012

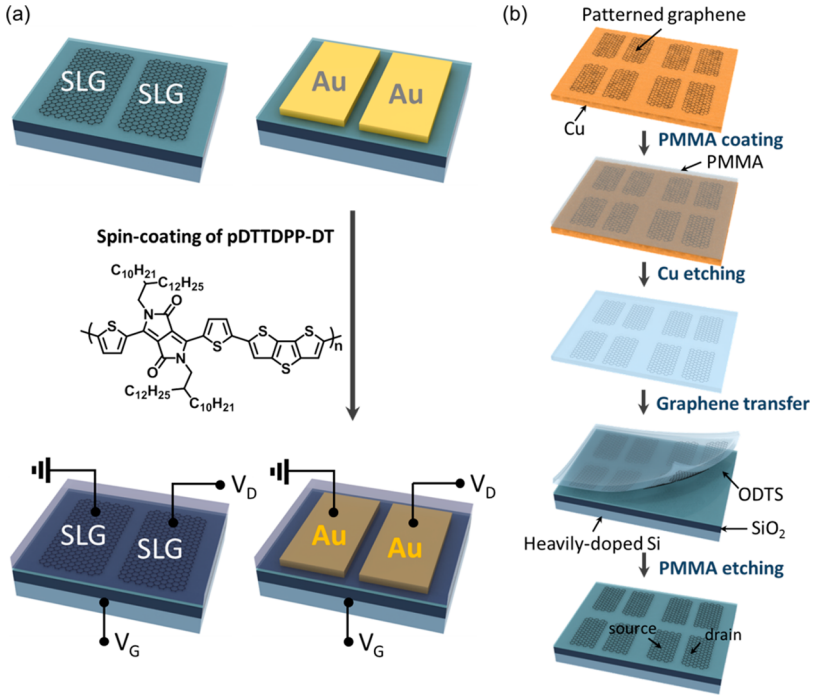

Figure 1. (a) Schematic diagram showing the fabrication of bottom-contact bottom-gate SLG- or Au-based transistors via spin-coating of the pDTTDPP-DT polymer onto the patterned SLG and Au electrodes. (b) Schematic diagram showing the steps taken to fabricate patterned CVD-grown SLG electrodes on the ODTS-coated SiO_2/Si wafer.

Cu metal catalyst was electrochemically etched using an aqueous 0.1 M ammonium persulfate solution. After Cu was etched, SLG source/drain electrode patterns supported by PMMA film were transferred on a ODTS-treated silicon water. For better intimate contact of the patterned SLG onto ODTS surface, the substrate was heated at 180 °C (above glass transition temperature of PMMA) for 30 min. PMMA layer was then removed by dipping in hot acetone. The thermal treatment of the patterned SLG/PMMA layer enhanced the yield of the SLG pattern transfer. The sheet resistance of the transferred SLG was 672 Ω/□, which is high enough to apply voltages and collect charge carriers in the transistors. Finally, a 50 nm thick pDTTDPP-DT film was deposited by spin-coating a 0.5 wt % polymer solution in chloroform onto the substrate. After spin-coating of the pDTTDPP-DT film, the samples were dried in a vacuum chamber (~10^{-3} Torr) for 24 h. The pDTTDPP-DT films were thermally annealed for 30 min in a vacuum chamber at different temperatures: 25, 100, 150, and 200 °C. The OFETs with Au electrodes that were patterned by masking were fabricated for comparison. The channel length (L) and width (W) of OFETs were 50 and 800 μm, respectively.

2.3. Measurements on Polymer Films and Substrates. The polymer films and electrode surfaces were imaged using AFM (XE-100, Park systems) in tapping mode. The electronic structures were acquired from UPS spectra acquired on a PHI 5000 Versaprobe spectrometer (Ulvac-PHI) equipped with a He I ($h\nu$ = 21.2 eV) radiation source. Photoemitted electrons were collected at normal emission with a pass energy of 2.95 eV at a base pressure of 6.7 × 10^{-8} Pa. All spectra were acquired at an applied bias of −9 V on the sample. Grazing incidence X-ray diffraction (GIXD) measurements were performed at the 3C and 9A beamline of the Pohang Light Source II (PLS II) in Korea. The wavelengths of X-ray were either 0.1165 or 0.1110 nm, and the incidence angle was chosen the angle between the critical angle of the sample and that of the substrate. The detectors used were CCD (model: Rayonix 2D SX165 or PI-SCX 4300). Water contact angles of the electrode substrates were measured using an automatic microscopic contact angle meter (PCA-1, Kyowa Interface Science). Prepared SLG Raman spectrum was taken on a confocal scanning Raman microscope (CRM 200, Witech). All theoretical calculations on molecular energy levels, surface plots, and geometries were carried out with the Gaussian 09 package. The ground-state geometries of all molecules have been fully optimized at the DFT level of theory with the three-parameter functional of Becke and the correlation functional of Lee et al. (B3LYP) using a standard 6-311G(d,p) basis set on all atoms.

3. RESULTS AND DISCUSSION

The solution-processable LBG polymer, pDTTDPP-DT, was synthesized via Stille polymerization[40,41] and purified by Soxhlet extraction using methanol, acetone, hexane, dichloromethane, and finally chloroform. The chemical structure is shown in Figure 1a, and the synthesis is described in detail in the Experimental Section. Note that the chloroform fraction of pDTTDPP-DT polymer contained a high amount of a very high molecular weight of M_n = 680 kDa with a polydispersity index (PDI = 2.55) and a low amount of a low molecular weight of M_n = 5.8 kDa with a polydispersity index (PDI = 1.61) (see gel permeation chromatogram shown in Supporting Information Figure S1). This dual molecular weight distribution was observed presumably because of the self-aggregation of high molecular weighted polymer chains. This was supported by the facts that (i) UV−visible absorption spectra of pDTTDPP-DT polymer solutions in *o*-dichlorobenzene at elevated temperatures were slightly blue-shifted and the absorption peak at 815 nm, associated with polymer interchain stacking, was significantly reduced (Supporting Information Figure S2a), and (ii) the UV−visible absorption features are nearly identical in three conditions: pDTTDPP-DT in *o*-dichlorobenzene solution, in chloroform solution (Supporting Information Figure S2b), and in film (Supporting Information Figure S3a). To clearly resolve the molecular weight of pDTTDPP-DT polymer, gel-permeation chromatography was again run with trichlorobenzene at 150 °C, which revealed M_n = 14 kDa with a PDI = 13.6 (Supporting Information Figure S4). Cyclic voltammetry (CV) revealed that the HOMO and LUMO levels were measured to be −5.18 and −3.33 eV,

DOI: 10.1021/acsami.5b00747
ACS Appl. Mater. Interfaces 2015, 7, 6002−6012

Table 1. Redox Potentials, HOMO/LUMO Levels, and Band Gaps of pDTTDPP-DT

	$E_{onset,ox}$ (V)	$E_{onset,red}$ (V)	HOMO[a] (eV)	LUMO[b] (eV)	$E_{g,cv}$[c] (eV)	$E_{g,opt}$[d] (eV)
pDTTDPP-DT	0.38	−1.47	−5.18	−3.33	1.85	1.44

[a]HOMO = $-(E_{onset,ox} + 4.8)$ eV. [b]LUMO = $-(E_{onset,red} + 4.8)$ eV. [c]$E_{g,cv}$= (LUMO − HOMO) eV. [d]$E_{g,opt}$ was determined from the onset of the UV−visible absorption spectra in film.

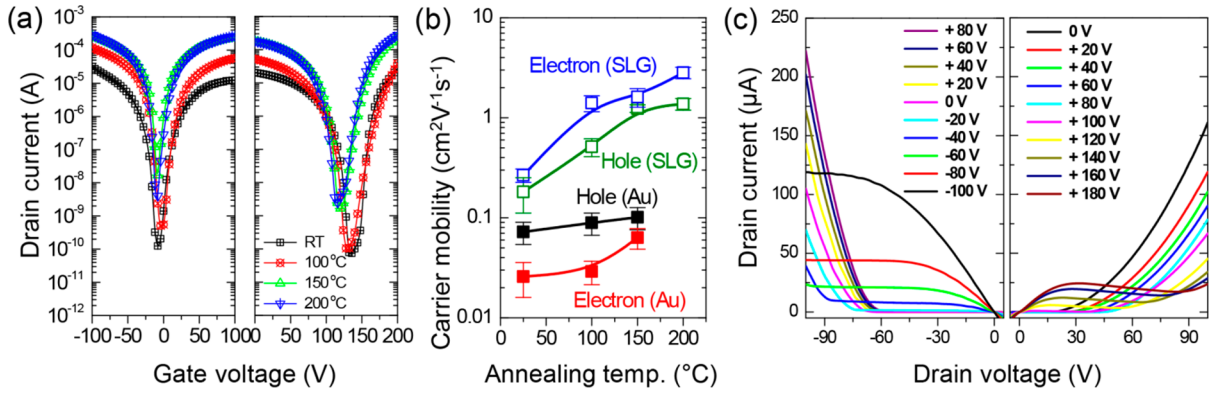

Figure 2. (a) Transfer characteristics at a fixed V_D of −80 or +80 V for OFETs prepared with SLG source/drain electrodes based on pDTTDPP-DT annealed at one of four temperatures: 25, 100, 150, and 200 °C. (b) Hole and electron mobilities of the pDTTDPP-DT OFETs prepared with SLG and Au source/drain electrodes, as a function of the pDTTDPP-DT annealing temperature. (c) Output characteristics of the OFETs prepared with SLG source/drain electrodes based on 200 °C-annealed pDTTDPP-DT films.

Table 2. Carrier Mobilities of the pDTTDPP-DT-Based OFETs with SLG or Au Source/Drain Electrodes at Various Annealing Temperatures[a]

electrode	carrier	25 °C	100 °C	150 °C	200 °C
Au	hole	0.08 ± 0.02	0.09 ± 0.02	0.10 ± 0.03	
	electron	0.02 ± 0.01	0.03 ± 0.01	0.06 ± 0.01	
SLG	hole	0.18 ± 0.07	0.51 ± 0.10	1.24 ± 0.11	1.38 ± 0.18
	electron	0.27 ± 0.04	1.41 ± 0.26	1.61 ± 0.34	2.82 ± 0.37

[a]Unit: $cm^2\ V^{-1}\ s^{-1}$.

respectively (Supporting Information Figure S3b). The electrochemical energy gap ($E_{g,cv}$) was 1.85 eV. Table 1 summarizes the optical and electrochemical properties. The molecular orbitals and geometry, obtained using density functional theory (DFT) calculations, suggested that both holes and electrons traveled easily along the planar polymer backbone through delocalized HOMO and LUMO orbitals (see below). The planar geometry and the sufficient spacing between the alkyl chains on the DPP units would facilitate close interchain stacking and interdigitation of the alkyl chains, yielding highly crystalline films.[29]

Figure 1b shows a schematic illustration of the steps involved in the fabrication of the CVD-grown SLG source−drain electrodes. In the first step, high-quality single-layer graphene was synthesized on a Cu foil, as described previously.[35,37] Supporting Information Figure S5 shows the Raman spectrum of the synthesized SLG. The graphene source/drain patterns were defined by photolithography using a commercial positive-type photoresist and oxygen plasma etching of the SLG layers on the Cu foil. Poly(methyl methacrylate) (PMMA) was spin-coated onto the patterned graphene on the Cu foil. The Cu metal catalyst was electrochemically etched using an aqueous 0.1 M ammonium persulfate solution. After etching Cu, SLG source/drain electrode patterns were transferred onto a silicon wafer with 300 nm thick thermally grown SiO_2 that were pretreated with octadecyltrichlorosilane (ODTS). The PMMA was then removed by hot acetone. Finally, a 50 nm thick pDTTDPP-DT film was deposited by spin-coating a chloroform solution containing the pDTTDPP-DT polymer (0.5 wt %) onto the ODTS-treated silicon wafer that was precoated with an array of SLG source/drain electrodes. The spin-coated polymer films were dried in a vacuum chamber for 24 h. The effects of thermal annealing on the OFET performance were examined by thermally annealing the pDTTDPP-DT films for 30 min in a vacuum chamber at one of four temperatures: 25, 100, 150, or 200 °C. For comparison, OFETs prepared with 40 nm thick Au electrodes were fabricated in the same manner, except that the electrodes were simply formed by thermally evaporating Au.

The electrical properties of the pDTTDPP-DT OFETs based on both the SLG and the Au source/drain electrodes were measured. Figure 2a and Supporting Information Figure S6 shows the transfer characteristics (drain current (I_D) vs gate voltage (V_G)) at drain voltages (V_D) of −80 or +80 V, for the OFETs prepared with SLG or Au electrodes, respectively. Both types of devices were annealed at various temperatures: 25 (as-spun), 100, 150, or 200 °C. Clear ambipolar charge transport behavior was observed in the hole-enhancement (V_D = −80 V) and electron-enhancement (V_D = +80 V) operational modes. The carrier mobilities (μ) of the devices were estimated in the respective saturation regimes according to the equation, $I_D = C_i \mu W (V_G - V_{th})^2/2L$, where C_i is the specific capacitance of the gate dielectric (11 nF/cm^2), μ is the carrier mobility, V_{th} is the threshold voltage, W is the channel width, and L is the channel length. As-spun pDTTDPP-DT OFETs prepared with Au electrodes exhibited average hole and electron mobilities of

DOI: 10.1021/acsami.5b00747
ACS Appl. Mater. Interfaces 2015, 7, 6002−6012

0.08(±0.02) and 0.02(±0.01) $cm^2\ V^{-1}\ s^{-1}$, respectively. By contrast, the as-spun pDTTDPP-DT OFETs prepared with the SLG electrodes yielded higher carrier mobilities: 0.18(±0.07) $cm^2\ V^{-1}\ s^{-1}$ for holes and 0.27(±0.04) $cm^2\ V^{-1}\ s^{-1}$ for electrons. Although thermal annealing of the pDTTDPP-DT films significantly increased the carrier mobilities for both the SLG and the Au-based OFET devices, as summarized in Figure 2b and Table 2, the SLG-based OFETs apparently outperformed the Au-based OFETs. The 150 °C-annealed pDTTDPP-DT films in the SLG-based OFETs yielded hole mobilities that exceeded a factor of 10 times corresponding values of the Au-based OFETs. The electron mobilities improved by more than a factor of 25 relative to the corresponding values obtained from the Au-based OFETs. The 200 °C-annealed pDTTDPP-DT OFETs prepared with SLG source/drain electrodes showed better average hole and electron mobilities of 1.38(±0.18) and 2.82(±0.37) $cm^2\ V^{-1}\ s^{-1}$, respectively. It should be also noted that the thermal annealing process enhanced the mobility in the SLG-based OFETs significantly as a function of annealing temperature, and the mobility of the 200 °C annealed pDTTDPP-DT film exceeded that of the as-spun polymer film by more than an order of magnitude. The high mobilities obtained from the SLG-based OFETs indicated well-balanced polarity and were among the highest values yet measured among ambipolar OFETs prepared simply from spin-coated semiconducting polymers.[14,17,25] The values obtained from the Au-based OFETs, on the other hand, were not high relative to the corresponding values obtained from previously reported OFETs incorporating semiconducting LBG polymers. The OFETs prepared with Au electrodes did not operate reliably upon thermal annealing at 200 °C due to the partial delamination of the pDTTDPP-DT film from the Au surface. Figure 2c shows the output characteristics (I_D vs V_D) associated with hole or electron accumulation in the 200 °C-annealed pDTTDPP-DT OFETs. These curves displayed typical ambipolar characteristics: diode-like behavior at a low gate bias and saturation behavior at a high gate bias.

The origin of the device's performance dependence on the electrode type and annealing temperature was explored by characterizing the thermally annealed pDTTDPP-DT films using ultraviolet photoelectron spectroscopy (UPS), grazing-incidence X-ray diffraction (GIXD), atomic force microscopy (AFM), and contact angle measurements (CA). First, UPS measurements were obtained to probe the energetic positions of the vacuum level (E_{vac}), Fermi level of the electrodes (E_{Fermi}), and HOMO level of pDTTDPP-DT relative to the E_{Fermi} of the electrodes upon contact between pDTTDPP-DT and the electrodes. The E_{vac} positions with respect to the E_{Fermi} of the electrodes were determined from the work function that corresponded to the difference between the He(I) source energy, that is, 21.2 eV, and the binding energy of the secondary electron cutoff. The HOMO levels of the thermally annealed pDTTDPP-DT films were estimated from the onsets of the photoelectron emission signal, and the LUMO levels were determined by considering the HOMO and $E_{g,cv}$ values. Figure 3a shows the secondary electron cutoff region of the UPS spectra of the electrode and pDTTDPP-DT/electrode films. The work functions of the Au, as-spun pDTTDPP-DT/Au, SLG, and as-spun pDTTDPP-DT/SLG surfaces were determined to be 5.24, 4.19, 4.52, and 4.09 eV, respectively. The work functions of the Au and SLG surfaces were consistent with the values reported previously.[37,42,43] These results

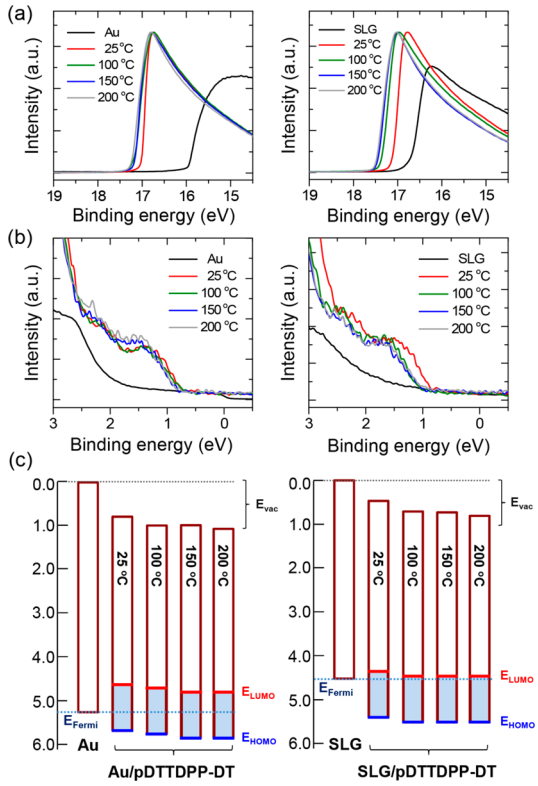

Figure 3. (a) UPS patterns near the secondary cutoff region, obtained from the 25 (as-spun), 100, 150, or 200 °C-annealed pDTTDPP-DT films prepared on the Au (left) or SLG (right) electrodes. (b) UPS patterns near the onset region, obtained from the 25 (as-spun), 100, 150, or 200 °C-annealed pDTTDPP-DT films prepared on the Au (left) or SLG (right) electrodes. (c) Alignment of the energy levels in the electrodes and pDTTDPP-DT film/electrode structures. The E_{LUMO} levels were estimated from the $E_{g,cv}$ and E_{HOMO} levels.

indicated that after applying the polymer coating onto each metal electrode, the vacuum level of the Au substrates tended to decrease (1.05 eV) to a greater extent than the vacuum level decrease observed in the SLG substrates (0.43 eV). Thermal annealing of the pDTTDPP-DT films decreased the work function slightly further. The different work functions (or vacuum levels) of the pDTTDPP-DT films and contact electrodes yielded significant differences in the HOMO/LUMO level alignment of pDTTDPP-DT with respect to the E_{Fermi} value for each contact electrode. Figure 3b shows the onset region of the UPS spectra obtained from Au, pDTTDPP-DT/Au, SLG, or pDTTDPP-DT/SLG. The spectra indicated that the HOMO levels of the pDTTDPP-DT films deposited onto either Au or SLG electrodes shifted to slightly deeper values upon thermal annealing, concomitant with the change in the vacuum levels. Figure 3c illustrates the relative alignments of the electrode Fermi levels and thermally annealed pDTTDPP-DT film energy levels. The pDTTDPP-DT/Au film had a lower ($E_{HOMO} - E_{Fermi}$) offset (0.81 eV) than the pDTTDPP-DT/SLG film (1.04 eV). This trend was consistent with the ($E_{HOMO} - E_{Fermi}$) offsets of the pentacene/Au (0.55 eV) and pentacene/SLG (0.7 eV) films measured by UPS.[37,44] Accordingly, the corresponding LUMO levels of the thermally annealed pDTTDPP-DT films on SLG had a lower ($E_{LUMO} - E_{Fermi}$) offset (0.81 eV) than the LUMO levels of the corresponding films on Au electrodes (1.04 eV). This energy offset trend appeared to be associated with the major charge

DOI: 10.1021/acsami.5b00747
ACS Appl. Mater. Interfaces 2015, 7, 6002−6012

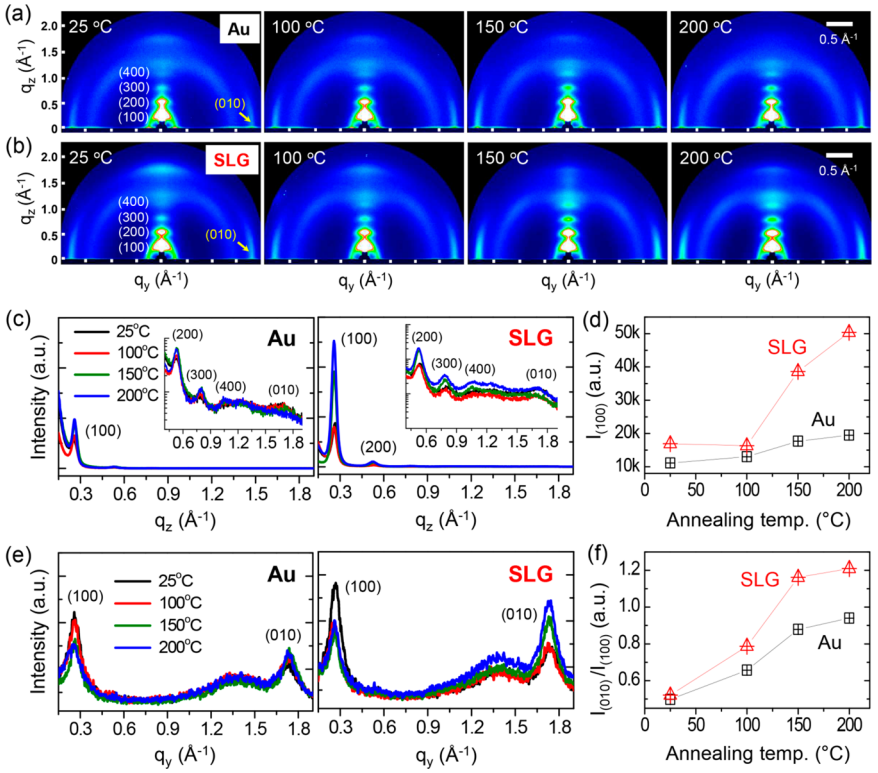

Figure 4. (a and b) GIXD patterns obtained from the 25 (as-spun), 100, 150, or 200 °C-annealed pDTTDPP-DT films prepared on the Au or SLG electrodes, respectively. (c) Out-of-plane X-ray diffraction profiles, extracted along the q_z direction at q_y = 0.00 Å^{-1}. The inset shows the semilog plots of the pDTTDPP-DT films prepared on the Au (left) or SLG (right) electrodes. (d) A plot of the intensity of the (100) peak along the out-of-plane direction versus the annealing temperature. (e) In-plane X-ray diffraction profiles, extracted along the q_y direction at q_z = 0.03 Å^{-1}. (f) The (010)/(100) intensity ratio in the in-plane direction as a function of the annealing temperature.

carrier transport type on the OFETs. In other words, the energy level alignment (i.e., carrier injection barrier height) might be related to the fact that the hole mobility is slightly higher for the Au-based OFETs and the electron mobilities are higher for the SLG-based OFETs.[2,7,17,32] On the other hand, note that the overall mobilities depended more strongly on the type of substrate and the annealing temperature, which suggests that, although the energetic barrier to carrier injection is indeed important for charge transport, there exists another transport-determining factor in the p-DTTDPP-DT OFETs. Thus, we investigated the packing and alignment of pDTTDPP-DT polymer chains on the surfaces of both the electrode and the gate dielectric.

The crystallinity of the thin pDTTDPP-DT film was investigated using synchrotron GIXD measurements to identify the effects of the surfaces of the source/drain electrodes, gate dielectric, and thermal annealing temperature on the polymer chain stacking and orientation. Figure 4a and b shows the GIXD images of the as-spun, 100, 150, and 200 °C-annealed pDTTDPP-DT films on the Au and SLG electrodes, respectively. In both of the electrode cases, the as-spun pDTTDPP-DT film exhibited strong (100) diffraction peaks along with second- and third-order peaks and a weak (010) reflection along the out-of-plane (q_z) direction. Upon thermal annealing of the pDTTDPP-DT film, the (h00) diffraction peak became more pronounced, and the (400) diffraction peak was more clearly observed along the q_z direction. The (010) peak along the q_y direction became intensified as compared to the weak (010) diffraction peak of the as-cast film, which is more pronounced on the SLG surface than on the Au surface.

The GIXD patterns were analyzed in detail by extracting the line-cut profiles along the q_z and q_y directions. Figure 4c shows the out-of-plane profiles, extracted along the q_z direction at q_y = 0.00 Å^{-1}, of the GIXD patterns of the pDTTDPP-DT films prepared on Au or SLG surfaces. The as-cast pDTTDPP-DT film on the Au surface showed strong (h00) diffraction peaks that corresponded to a $d_{(h00)}$ spacing of 23.0 Å. The (h00) diffraction peak intensity increased and the out-of-plane spacing increased slightly to 23.2 Å upon annealing at 200 °C (left-hand side of Figure 4c). The as-cast pDTTDPP-DT film on the SLG surface displayed a slightly higher crystallinity than the corresponding film cast onto Au surface, and the (h00) diffraction peaks corresponded to a $d_{(h00)}$ spacing of 23.0 Å. Thermal annealing resulted in even stronger (h00) diffraction peaks, and the out-of-plane spacing increased further to 23.6 Å for 200 °C (right-hand side of Figure 4c). Figure 4d plots the dependence of the (100) diffraction peak intensity on the annealing temperature and the type of contact electrode. Figure 4e shows the in-plane profiles of the GIXD patterns of the pDTTDPP-DT films prepared on the Au or SLG surfaces, extracted along the q_y direction at q_z = 0.03 Å^{-1}. Thermal annealing resulted in a significant increase in the in-plane (010) peak intensity and a decrease in the in-plane (100) diffraction peak profile. The (010) peaks measured from the electrode surfaces indicated nearly identical π–π stacking distances of 3.63 Å. It should be noted that (i) this π–π distance was among the smallest distance observed among the LBG polymers,[8,10,11,13,17,25] possibly due to the planar backbone conformation, and (ii) the other (010) peak intensity increased significantly and the (100) peaks decreased in the in-plane

DOI: 10.1021/acsami.5b00747
ACS Appl. Mater. Interfaces 2015, 7, 6002–6012

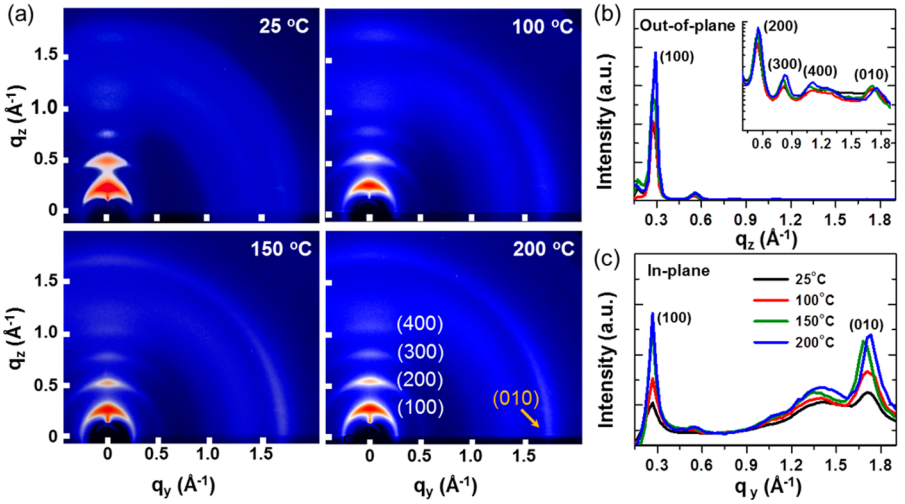

Figure 5. (a) GIXD patterns obtained from the 25, 100, 150, or 200 °C-annealed pDTTDPP-DT films prepared on the gate dielectric. (b) Out-of-plane X-ray diffraction profiles extracted along the q_z direction at q_y = 0.00 Å^{-1}. The inset shows the enlarged (200), (300), (400), and (010) peaks. (c) In-plane X-ray diffraction profiles along the q_y direction at q_z = 0.03 Å^{-1}.

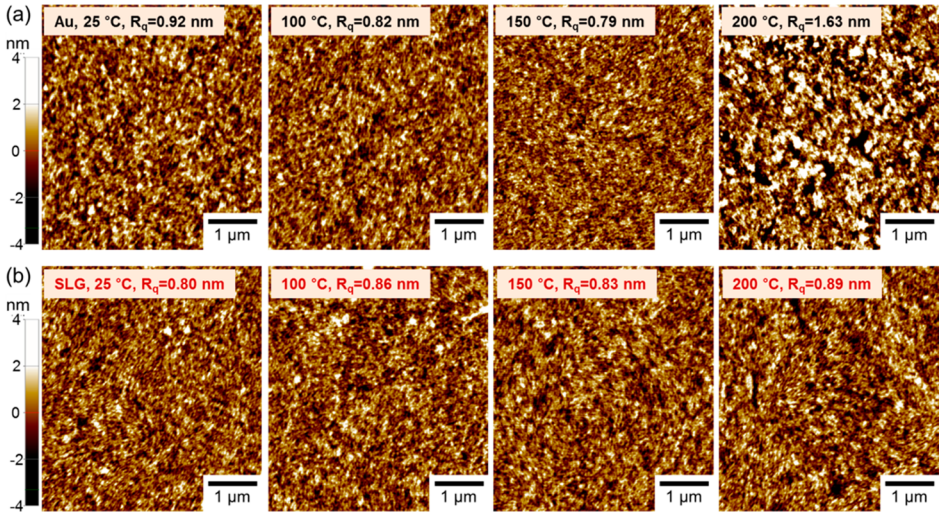

Figure 6. (a and b) AFM topographic images of 25 (as-spun), 100, 150, or 200 °C-annealed pDTTDPP-DT films prepared on the Au or SLG electrodes, respectively.

profiles obtained from the pDTTDPP-DT films prepared on the SLG surface. Accordingly, the ratio between the (010) intensity and the (100) intensity in the in-plane direction increased (Figure 4f). The structural improvement was larger in the film prepared on the SLG electrode. It should be emphasized that the very strong (100) peak in the out-of-plane direction and the pronounced (010) peak in the in-plane direction obtained from the pDTTDPP-DT film prepared on the SLG surface and annealed at 200 °C reflected that the pDTTDPP-DT polymer chains were extensively stacked, with good long-range ordering. In summary, the GIXD analysis on the pDTTDPP-DT films on the electrodes indicated that the crystallinity of the pDTTDPP-DT polymer films improved significantly with increasing annealing temperature and the fraction of molecules having an edge-on orientation increased. These features were shown on the SLG substrates more obviously than on the Au substrates. Importantly, note that the edge-on oriented highly crystalline chain packing motif was important to the continuous crystalline domain growth of the polymers in the interfacial region between the electrodes and the channel, which was beneficial for charge injection and transport.

The crystallinity of the thin pDTTDPP-DT film in the channel region was also investigated to examine how the polymer chain packing and orientation depended on the presence of ODTS-coated SiO_2/Si gate dielectric surfaces or the thermal annealing temperature. Figure 5a shows the GIXD images of the as-spun 100, 150, and 200 °C-annealed pDTTDPP-DT films prepared on the ODTS-coated SiO_2/Si surface. Figure 5b and c shows, respectively, the out-of-plane profiles extracted along the q_z direction at q_y = 0.00 Å^{-1} and the in-plane profiles extracted along the q_y direction at q_z = 0.03 Å^{-1}. The main features of the pDTTDPP-DT films on the ODTS-coated SiO_2/Si surface were closer to those of the pDTTDPP-DT films on the SLG surface, based on the fact that as the annealing temperature increased, pDTTDPP-DT films displayed the increased (100) diffraction peak with high-order peaks along the q_z direction and also the intensified (010) diffraction peak along the q_y direction in a similar incremental pattern of crystalline peaks. The 200 °C-annealed pDTTDPP-

DOI: 10.1021/acsami.5b00747
ACS Appl. Mater. Interfaces 2015, 7, 6002−6012

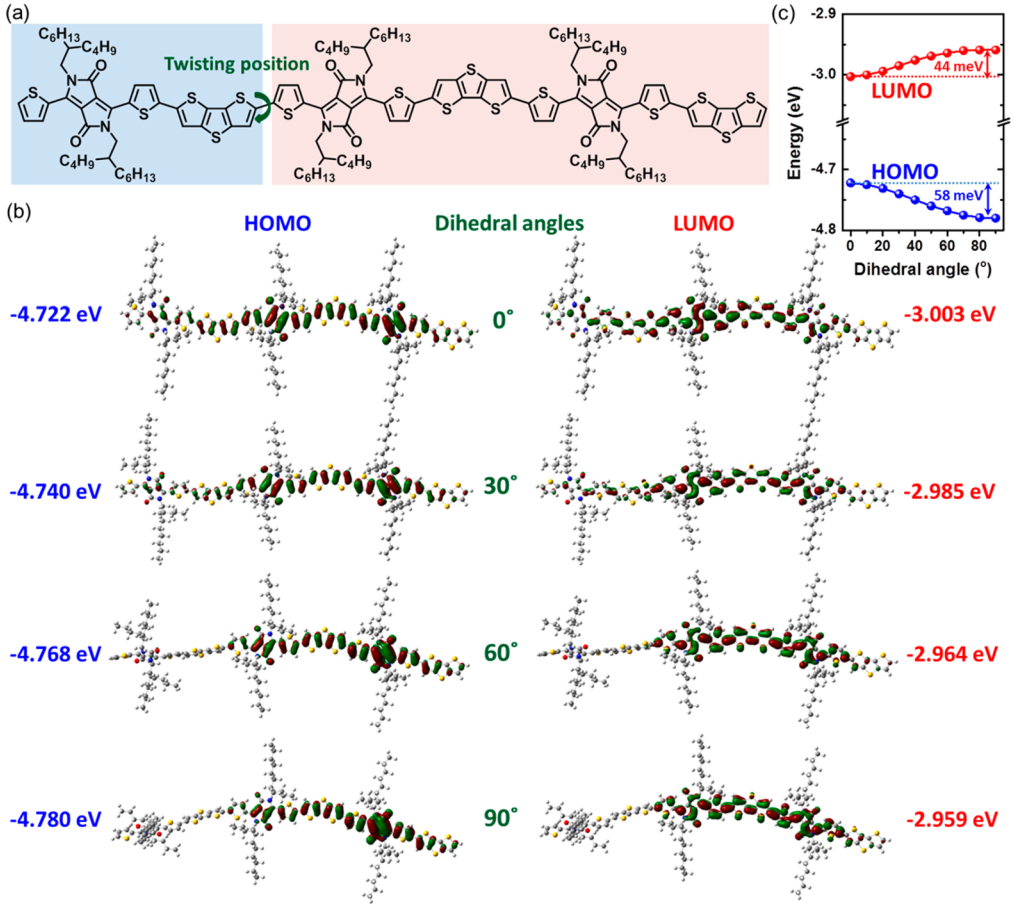

Figure 7. (a) The structure of a DTTDPP-BO trimer, a model compound for the pDTTDPP-DT polymer. The arrow indicates the position at which the two molecular planes twisted. (b) HOMO/LUMO levels and their orbitals at representative dihedral angles of 0°, 30°, 60°, and 90°. (c) The dependence of the HOMO/LUMO levels on the dihedral angle.

DT film displayed an out-of-plane spacing of 23.4 Å with a $\pi-\pi$ stacking distance of 3.63 Å. The similarities between the polymer films prepared on the SLG and on the channel region surfaces might result from the lower surface roughness and low surface energy of the SLG surface, as observed in the surface images and contact angle measurements collected from the substrates; AFM imaging revealed that the SLG electrode surface was 3 times smoother than the bare Au electrode surface (images are shown in Supporting Information Figure S7), and the water contact angles were found to be 47° and 82° for the Au and SLG substrates, respectively. It is possible that the hydrophobic SLG surface interacted strongly with the hydrophobic regions of the pDTTDPP-DT polymer alkyl chains, and the alkyl chains assembled more easily on the flat SLG surface to guide the self-organization of the polymer backbone and the stacking of neighboring polymer chains. It should be noted that the structural similarities between the polymer films prepared on the SLG electrodes and on the gate dielectric suggested that the interfaces between polymer domains formed on both of the surfaces can be better glued, and thus efficient charge transport can be attainable through the well-ordered close $\pi-\pi$ stacking interactions between the SLG electrode and the channel region.[37,45]

The surface morphologies of the as-spun, 100, 150, and 200 °C-annealed pDTTDPP-DT films were examined using AFM. Figure 6 presents the topographic images of the corresponding films. The as-spun pDTTDPP-DT film prepared on the Au surface displayed crystalline but somewhat aggregated granular surfaces, whereas the as-spun pDTTDPP-DT film prepared on the SLG surface displayed more uniform and better connected fibrous polymer domains. The 25, 100, and 150 °C-annealed pDTTDPP-DT films displayed similarly a fibrous polymer morphology with low rms values. The 200 °C-annealed pDTTDPP-DT films prepared on the Au surface, however, included aggregates and yielded doubly rougher surfaces than any of the other polymer films. The poor morphologies of the films prepared on Au surfaces and annealed at 200 °C were correlated with both partial delamination and unstable electrical properties in the 200 °C-annealed pDTTDPP-DT OFETs based on Au source/drain electrodes. The 200 °C-annealed pDTTDPP-DT films prepared on the SLG surfaces conserved the smooth morphology with the fibrous crystalline feature, similar to the films annealed at the other temperatures. This stable interface between the pDTTDPP-DT films and the SLG surface allowed us to broaden the range of film annealing temperatures and achieve the superior hole and electron mobilities to the corresponding values obtained OFET devices prepared on Au surface. Collectively, the GIXD and AFM results revealed that the substrate type and application of thermal annealing strongly impacted both the crystalline microstructure and the molecular morphology of the films, and the 200 °C-annealed pDTTDPP-DT film prepared on the SLG electrodes displayed an optimal morphology, yielding high-performance ambipolar OFETs.

DOI: 10.1021/acsami.5b00747
ACS Appl. Mater. Interfaces 2015, 7, 6002−6012

Finally, we investigated the mechanism by which the electron mobility improved to a greater extent than did the hole mobility in the SLG-based OFETs at higher thermal annealing temperatures, even though both mobilities increased as a result of the improved polymer film crystallinity. First, the electron injection barrier decreased slightly further during thermal annealing, whereas the hole injection barrier increased slightly, as revealed by the UPS data. This fact has affected in part the increase in the electron mobility. Second, the potential effect of polymer backbone twist on charge carrier transport was examined by simulating molecular geometries and intramolecular orbital overlapping using density-functional-theory (DFT) calculations. We considered this effect because some fractions of polymer backbone twists can exist, especially in the polymer chains connecting the crystalline domains, while the film crystallinity improved and the polymer chains formed long-range ordered domains with an edge-on orientation upon thermal annealing, and these backbone twists could hamper the intra- and interchain charge transports. The effects of the backbone twists on the molecular orbital overlap and energy levels were investigated by monitoring the HOMO/LUMO orbitals of a model compound, $(T\text{-}DTT\text{-}T\text{-}DTT)_3$, where T stands for thiophene. The 2-butyloctyl groups were employed as alkyl side chains in place of 2-decyltetradecyl groups to save calculation time. The chemical structure is shown in Figure 7a. For a simplest case, the molecule was twisted with a dihedral angle in the middle of the molecule that was varied from 10° to 90°, while the other regions of the molecular geometries were assumed to be fixed. Figure 7b illustrates the geometries and surface plots of the HOMO/LUMO orbitals with representative dihedral angles of 0°, 30°, 60°, and 90° (Supporting Information Figure S8 shows the full geometries and surface plots of the HOMO/LUMO orbitals with a variation of dihedral angles change between 0° and 90°). Larger dihedral angles disrupted the electronic delocalization across the two halves of the molecule, as indicated in Figure 7b, and reduced the contributions of the shorter left-hand side of the molecule to charge transport. At the same time, the HOMO orbitals in the longer right-hand side of the molecule became rather localized around the far right DPP moiety, whereas the LUMO orbitals retained a well-distributed LUMO orbital system. Moreover, Figure 7c presents the dependence of each energy level on the dihedral angle. As the dihedral angle increased, the HOMO levels deepened to a greater extent than the destabilization of LUMO levels. As an extreme case, the 90° backbone twist can lower HOMO by 58 meV and raise LUMO by 44 meV. In sum, the molecular simulation results suggested that electron transport would be less deterred by the partial twists of the pDTTDPP-DT backbone. In other words, the better orbital overlapping and less energetic change in the LUMO could provide a tentative explanation for the good electron mobility observed in the ambipolar OFETs based on the pDTTDPP-DT.

4. CONCLUSIONS

We synthesized a low band gap pDTTDPP-DT polymer containing electron-rich DTT units and electron-deficient DPP units and characterized its electrical properties in a transistor format using SLG or Au source/drain electrodes. The mobilities measured in OFETS prepared using the SLG electrodes were more than 10 times the corresponding values measured in OFETs prepared using typical Au electrodes. Moreover, thermal annealing of the semiconducting film effectively enhanced the carrier mobilities within the pDTTDPP-DT films. The optimized ambipolar OFETs prepared with SLG electrodes exhibited the average hole and electron mobilities of 1.38 and 2.82 $cm^2\ V^{-1}\ s^{-1}$, respectively, while the OFETs prepared with Au electrodes displayed the average hole and electron mobilities of 0.10 and 0.06 $cm^2\ V^{-1}\ s^{-1}$, respectively. Full characterization of films revealed that the pDTTDPP-DT films on the SLG electrode displayed a better optimal energy level alignment for the ambipolar behavior and became highly crystalline with an edge-on orientation as a function of annealing temperature. These characteristics explained the superior carrier transport in the SLG-based OFET than in the Au-based OFET. Overall, this work demonstrates the strong dependence of ambipolar carrier transport on the source/drain electrode and annealing temperature and highlights the importance of SLG electrodes to the preparation of high-performance ambipolar OFETs.

■ ASSOCIATED CONTENT

Supporting Information

Synthesis and characterization of pDTTDPP-DT polymer, Raman spectrum of the SLG, AFM images of Au and SLG surface, and the dependence of molecular orbitals on the dihedral angles. This material is available free of charge via the Internet at http://pubs.acs.org.

■ AUTHOR INFORMATION

Corresponding Authors

*Tel.: +82 31 299 4165. Fax: +82 31 299 4119. E-mail: jhcho94@skku.edu.

*Tel.: +82 2 958 5516. Fax: +82 2 958 6649. E-mail: bongsoo@kist.re.kr.

Author Contributions

□J.Y.C. and W.K. contributed equally.

Notes

The authors declare no competing financial interest.

■ ACKNOWLEDGMENTS

This work was supported by the New and Renewable Energy Program of the Korea Institute of Energy Technology Evaluation and Planning (KETEP) grant funded by the Korea Goverment Ministry of Trade, Industry & Energy (MTIE) (20133030000130, 20113030010030), by the Korea Institute of Science and Technology (KIST) Internal Project, by the National Research Foundation of Korea Grant funded by the Korean Government (MSIP) (2013, University-Institute corporation program), and Basic Science Research Program (2009-0083540) of the National Research Foundation of Korea (NRF) funded by the Ministry of Education, Science and Technology, and the World-Class 300 Project (Development of organic materials with high transmittance, high insulating properties, and high flexibility for next generation display) funded by the Small and Medium Business Administration (SMBA) in Korea.

■ REFERENCES

(1) Bisri, S. Z.; Piliego, C.; Gao, J.; Loi, M. A. Outlook and Emerging Semiconducting Materials for Ambipolar Transistors. *Adv. Mater.* **2014**, *26*, 1176−1199.

(2) Zaumseil, J.; Sirringhaus, H. Electron and Ambipolar Transport in Organic Field-Effect Transistors. *Chem. Rev.* **2007**, *107*, 1296−1323.

DOI: 10.1021/acsami.5b00747
ACS Appl. Mater. Interfaces 2015, 7, 6002−6012

(3) Yan, H.; Chen, Z.; Zheng, Y.; Newman, C.; Quinn, J. R.; Dotz, F.; Kastler, M.; Facchetti, A. A High-Mobility Electron-Transporting Polymer for Printed Transistors. *Nature* **2009**, *457*, 679−686.
(4) Kang, M. S.; Frisbie, C. D. A Pedagogical Perspective on Ambipolar FETs. *ChemPhysChem* **2013**, *14*, 1547−1552.
(5) Zhang, X.; Richter, L. J.; DeLongchamp, D. M.; Kline, R. J.; Hammond, M. R.; McCulloch, I.; Heeney, M.; Ashraf, R. S.; Smith, J. N.; Anthopoulos, T. D.; Schroeder, B.; Geerts, Y. H.; Fischer, D. A.; Toney, M. F. Molecular Packing of High-Mobility Diketo Pyrrolo-Pyrrole Polymer Semiconductors with Branched Alkyl Side Chains. *J. Am. Chem. Soc.* **2011**, *133*, 15073−15084.
(6) Liu, X.; Guo, Y.; Ma, Y.; Chen, H.; Mao, Z.; Wang, H.; Yu, G.; Liu, Y. Flexible, Low-Voltage and High-Performance Polymer Thin-Film Transistors and Their Application in Photo/Thermal Detectors. *Adv. Mater.* **2014**, *26*, 3631−3636.
(7) Yun, H.-J.; Lee, G. B.; Chung, D. S.; Kim, Y.-H.; Kwon, S.-K. Novel Diketopyrroloppyrrole Random Copolymers: High Charge-Carrier Mobility From Environmentally Benign Processing. *Adv. Mater.* **2014**, *26*, 6612−6616.
(8) Kang, I.; Yun, H.-J.; Chung, D. S.; Kwon, S.-K.; Kim, Y.-H. Record High Hole Mobility in Polymer Semiconductors via Side-Chain Engineering. *J. Am. Chem. Soc.* **2013**, *135*, 14896−14899.
(9) Kronemeijer, A. J.; Gili, E.; Shahid, M.; Rivnay, J.; Salleo, A.; Heeney, M.; Sirringhaus, H. A Selenophene-Based Low-Bandgap Donor−Acceptor Polymer Leading to Fast Ambipolar Logic. *Adv. Mater.* **2012**, *24*, 1558−1565.
(10) Mei, J.; Kim, D. H.; Ayzner, A. L.; Toney, M. F.; Bao, Z. Siloxane-Terminated Solubilizing Side Chains: Bringing Conjugated Polymer Backbones Closer and Boosting Hole Mobilities in Thin-Film Transistors. *J. Am. Chem. Soc.* **2011**, *133*, 20130−20133.
(11) Kim, G.; Kang, S.-J.; Dutta, G. K.; Han, Y.-K.; Shin, T. J.; Noh, Y.-Y.; Yang, C. A Thienoisoindigo-Naphthalene Polymer with Ultrahigh Mobility of 14.4 $cm^2/V{\cdot}s$ That Substantially Exceeds Benchmark Values for Amorphous Silicon Semiconductors. *J. Am. Chem. Soc.* **2014**, *136*, 9477−9483.
(12) Lei, T.; Dou, J.-H.; Pei, J. Influence of Alkyl Chain Branching Positions on the Hole Mobilities of Polymer Thin-Film Transistors. *Adv. Mater.* **2012**, *24*, 6457−6461.
(13) Tsao, H. N.; Cho, D. M.; Park, I.; Hansen, M. R.; Mavrinskiy, A.; Yoon, D. Y.; Graf, R.; Pisula, W.; Spiess, H. W.; Müllen, K. Ultrahigh Mobility in Polymer Field-Effect Transistors by Design. *J. Am. Chem. Soc.* **2011**, *133*, 2605−2612.
(14) Lei, T.; Dou, J.-H.; Ma, Z.-J.; Yao, C.-H.; Liu, C.-J.; Wang, J.-Y.; Pei, J. Ambipolar Polymer Field-Effect Transistors Based on Fluorinated Isoindigo: High Performance and Improved Ambient Stability. *J. Am. Chem. Soc.* **2012**, *134*, 20025−20028.
(15) Shin, J.; Hong, T. R.; Lee, T. W.; Kim, A.; Kim, Y. H.; Cho, M. J.; Choi, D. H. Template-Guided Solution-Shearing Method for Enhanced Charge Carrier Mobility in Diketopyrrolopyrrole-Based Polymer Field-Effect Transistors. *Adv. Mater.* **2014**, *26*, 6031−6035.
(16) Chen, H.; Guo, Y.; Yu, G.; Zhao, Y.; Zhang, J.; Gao, D.; Liu, H.; Liu, Y. Highly π-Extended Copolymers with Diketopyrrolopyrrole Moieties for High-Performance Field-Effect Transistors. *Adv. Mater.* **2012**, *24*, 4618−4622.
(17) Sun, B.; Hong, W.; Yan, Z.; Aziz, H.; Li, Y. Record High Electron Mobility of 6.3 $cm^2V^{-1}s^{-1}$ Achieved for Polymer Semiconductors Using a New Building Block. *Adv. Mater.* **2014**, *26*, 2636−2642.
(18) Kim, J.; Han, A. R.; Hong, J.; Kim, G.; Lee, J.; Shin, T. J.; Oh, J. H.; Yang, C. Ambipolar Semiconducting Polymers with π-Spacer Linked Bis-Benzothiadiazole Blocks as Strong Accepting Units. *Chem. Mater.* **2014**, *26*, 4933−4942.
(19) Tseng, H.-R.; Ying, L.; Hsu, B. B. Y.; Perez, L. A.; Takacs, C. J.; Bazan, G. C.; Heeger, A. J. High Mobility Field Effect Transistors Based on Macroscopically Oriented Regioregular Copolymers. *Nano Lett.* **2012**, *12*, 6353−6357.
(20) Luo, C.; Kyaw, A. K. K.; Perez, L. A.; Patel, S.; Wang, M.; Grimm, B.; Bazan, G. C.; Kramer, E. J.; Heeger, A. J. General Strategy for Self-Assembly of Highly Oriented Nanocrystalline Semiconducting Polymers with High Mobility. *Nano Lett.* **2014**, *14*, 2764−2771.
(21) Tseng, H.-R.; Phan, H.; Luo, C.; Wang, M.; Perez, L. A.; Patel, S. N.; Ying, L.; Kramer, E. J.; Nguyen, T.-Q.; Bazan, G. C.; Heeger, A. J. High-Mobility Field-Effect Transistors Fabricated with Macroscopic Aligned Semiconducting Polymers. *Adv. Mater.* **2014**, *26*, 2993−2998.
(22) Luzio, A.; Fazzi, D.; Nübling, F.; Matsidik, R.; Straub, A.; Komber, H.; Giussani, E.; Watkins, S. E.; Barbatti, M.; Thiel, W.; Gann, E. H.; Thomsen, L.; McNeill, C. R.; Caironi, M.; Sommer, M. Structure-Function Relationships of High-Electron Mobility Naphthalene Diimide Copolymers Prepared by Direct Arylation. *Chem. Mater.* **2014**, *26*, 6233−6240.
(23) Kim, R.; Amegadze, P. S. K.; Kang, I.; Yun, H.-J.; Noh, Y.-Y.; Kwon, S.-K.; Kim, Y.-H. High-Mobility Air-Stable Naphthalene Diimide-Based Copolymer Containing Extended π-Conjugation for n-Channel Organic Field Effect Transistors. *Adv. Funct. Mater.* **2013**, *23*, 5719−5727.
(24) Guo, X.; Kim, F. S.; Seger, M. J.; Jenekhe, S. A.; Watson, M. D. Naphthalene Diimide-Based Polymer Semiconductors: Synthesis, Structure−Property Correlations, and n-Channel and Ambipolar Field-Effect Transistors. *Chem. Mater.* **2012**, *24*, 1434−1442.
(25) Lee, J.; Han, A. R.; Yu, H.; Shin, T. J.; Yang, C.; Oh, J. H. Boosting the Ambipolar Performance of Solution-Processable Polymer Semiconductors via Hybrid Side-Chain Engineering. *J. Am. Chem. Soc.* **2013**, *135*, 9540−9547.
(26) Lei, T.; Wang, J.-Y.; Pei, J. Roles of Flexible Chains in Organic Semiconducting Materials. *Chem. Mater.* **2013**, *26*, 594−603.
(27) Facchetti, A. π-Conjugated Polymers for Organic Electronics and Photovoltaic Cell Applications. *Chem. Mater.* **2010**, *23*, 733−758.
(28) Yun, H.-J.; Choi, H. H.; Kwon, S.-K.; Kim, Y.-H.; Cho, K. Conformation-Insensitive Ambipolar Charge Transport in a Diketo-pyrrolopyrrole-Based Co-polymer Containing Acetylene Linkages. *Chem. Mater.* **2014**, *26*, 3928−3937.
(29) Lee, J. S.; Son, S. K.; Song, S.; Kim, H.; Lee, D. R.; Kim, K.; Ko, M. J.; Choi, D. H.; Kim, B.; Cho, J. H. Importance of Solubilizing Group and Backbone Planarity in Low Band Gap Polymers for High Performance Ambipolar field-effect Transistors. *Chem. Mater.* **2012**, *24*, 1316−1323.
(30) Mei, J.; Bao, Z. Side Chain Engineering in Solution-Processable Conjugated Polymers. *Chem. Mater.* **2013**, *26*, 604−615.
(31) An, T. K.; Kang, I.; Yun, H.-j.; Cha, H.; Hwang, J.; Park, S.; Kim, J.; Kim, Y. J.; Chung, D. S.; Kwon, S.-K.; Kim, Y.-H.; Park, C. E. Solvent Additive to Achieve Highly Ordered Nanostructural Semi-crystalline DPP Copolymers: Toward a High Charge Carrier Mobility. *Adv. Mater.* **2013**, *25*, 7003−7009.
(32) Dimitrakopoulos, C. D.; Malenfant, P. R. L. Organic Thin Film Transistors for Large Area Electronics. *Adv. Mater.* **2002**, *14*, 99−117.
(33) Lee, W. H.; Park, J.; Sim, S. H.; Jo, S. B.; Kim, K. S.; Hong, B. H.; Cho, K. Transparent Flexible Organic Transistors Based on Monolayer Graphene Electrodes on Plastic. *Adv. Mater.* **2011**, *23*, 1752−1756.
(34) Lee, S.-K.; Kim, B. J.; Jang, H.; Yoon, S. C.; Lee, C.; Hong, B. H.; Rogers, J. A.; Cho, J. H.; Ahn, J.-H. Stretchable Graphene Transistors with Printed Dielectrics and Gate Electrodes. *Nano Lett.* **2011**, *11*, 4642−4646.
(35) Kim, K. S.; Zhao, Y.; Jang, H.; Lee, S. Y.; Kim, J. M.; Kim, K. S.; Ahn, J.-H.; Kim, P.; Choi, J.-Y.; Hong, B. H. Large-Scale Pattern Growth of Graphene Films for Stretchable Transparent Electrodes. *Nature* **2009**, *457*, 706−710.
(36) Li, X.; Cai, W.; An, J.; Kim, S.; Nah, J.; Yang, D.; Piner, R.; Velamakanni, A.; Jung, I.; Tutuc, E.; Banerjee, S. K.; Colombo, L.; Ruoff, R. S. Large-Area Synthesis of High-Quality and Uniform Graphene Films on Copper Foils. *Science* **2009**, *324*, 1312−1314.
(37) Lee, W. H.; Park, J.; Sim, S. H.; Lim, S.; Kim, K. S.; Hong, B. H.; Cho, K. Surface-Directed Molecular Assembly of Pentacene on Monolayer Graphene for High-Performance Organic Transistors. *J. Am. Chem. Soc.* **2011**, *133*, 4447−4454.
(38) Lee, S.; Jo, G.; Kang, S.-J.; Wang, G.; Choe, M.; Park, W.; Kim, D.-Y.; Kahng, Y. H.; Lee, T. Enhanced Charge Injection in Pentacene

DOI: 10.1021/acsami.5b00747
ACS Appl. Mater. Interfaces 2015, 7, 6002−6012

Field-Effect Transistors with Graphene Electrodes. *Adv. Mater.* **2011**, *23*, 100−105.
(39) Jang, J.; Park, J.; Nam, S.; Anthony, J. E.; Kim, Y.; Kim, K. S.; Kim, K. S.; Hong, B. H.; Park, C. E. Self-Organizing Properties of Triethylsilylethynyl-Anthradithiophene on Monolayer Graphene Electrodes in Solution-Processed Transistors. *Nanoscale* **2013**, *5*, 11094−11101.
(40) Ryu, T. I.; Yoon, Y.; Kim, J.-H.; Hwang, D.-H.; Ko, M. J.; Lee, D.-K.; Kim, J. Y.; Kim, H.; Park, N.-G.; Kim, B.; Son, H. J. Simultaneous Enhancement of Solar Cell Efficiency and Photostability via Chemical Tuning of Electron Donating Units in Diketopyrrolopyrrole-Based Push−Pull Type Polymers. *Macromolecules* **2014**, *47*, 6270−6280.
(41) Jung, J. W.; Liu, F.; Russell, T. P.; Jo, W. H. A High Mobility Conjugated Polymer Based on Dithienothiophene and Diketopyrrolopyrrole for Organic Photovoltaics. *Energy Environ. Sci.* **2012**, *5*, 6857−6861.
(42) Kim, B.; Choi, S. H.; Zhu, X. Y.; Frisbie, C. D. Molecular Tunnel Junctions Based on π-Conjugated Oligoacene Thiols and Dithiols between Ag, Au, and Pt Contacts: Effect of Surface Linking Group and Metal Work Function. *J. Am. Chem. Soc.* **2011**, *133*, 19864−19877.
(43) Kim, J.-H.; Hwang, J. H.; Suh, J.; Tongay, S.; Kwon, S.; Hwang, C. C.; Wu, J.; Park, J. Y. Work Function Engineering of Single Layer Graphene by Irradiation-Induced Defects. *Appl. Phys. Lett.* **2013**, *103*, 171604.
(44) Schroeder, P. G.; France, C. B.; Park, J. B.; Parkinson, B. A. Orbital Alignment and Morphology of Pentacene Deposited on Au(111) and SnS2 Studied Using Photoemission Spectroscopy. *J. Phys. Chem. B* **2003**, *107*, 2253−2261.
(45) Basu, S.; Lee, M. C.; Wang, Y.-H. Graphene-Based Electrodes for Enhanced Organic Thin Film Transistors Based on Pentacene. *Phys. Chem. Chem. Phys.* **2014**, *16*, 16701−16710.

DOI: 10.1021/acsami.5b00747
ACS Appl. Mater. Interfaces 2015, 7, 6002−6012